

1 **Ultrahigh-resolution FT-ICR mass spectrometry characterization of α -pinene** 2 **ozonolysis SOA**

3 Annie L. Putman¹, John H. Offenberg², Rebeka Fisseha³, Shuvashish Kundu¹, Thom A. Rahn³ and
4 Lynn R. Mazzoleni^{1,4*}

5 ¹Michigan Technological University, Department of Chemistry, Houghton, MI 49931, USA

6 ²U.S. Environmental Protection Agency, National Exposure Research Laboratory, Human Exposure Atmospheric Sciences
7 Division, Research Triangle Park, NC 27711, USA

8 ³Los Alamos National Laboratory, Earth and Environmental Sciences, Los Alamos, NM 87545, USA

9 ⁴Michigan Technological University, Atmospheric Sciences Program, Houghton, MI 49931, USA

10 *Corresponding author. Email: lrmazzol@mtu.edu, Phone 1-906-487-1853, Fax 1-906-487-2061

11 Submitted to Atmospheric Environment on April 21, 2011; Revised August 31, 2011; Accepted October 3, 2011.

12 **Abstract**

13 Secondary organic aerosol (SOA) of α -pinene ozonolysis with and without hydroxyl radical scavenging
14 hexane was characterized by ultrahigh-resolution Fourier transform ion cyclotron resonance mass
15 spectrometry (FT ICR MS). Molecular formulas for more than 900 negative ions were identified over the
16 mass range of 100 to 850 u. Hydroxyl radicals formed during the ozonolysis of α -pinene might be
17 expected to alter the composition of SOA, however a majority of the molecular formulas were identified
18 in all three experiments and with a few exceptions they had similar relative abundances. Thus, the
19 detailed composition of SOA was only slightly influenced by the presence or absence of hydroxyl radical
20 scavenging hexane. The negative ion mass spectra of the SOA contained four groups of peaks with
21 increasing mass spectral complexity corresponding to increasing molecular weight. The mean values of
22 O:C decreased from 0.55 to 0.42 with increasing molecular weight, but the mean value of H:C,
23 approximately 1.5, did not change with increasing molecular weight. The molecular formulas with the
24 highest relative abundances in Group I and II contained 5-7 and 7-10 oxygen atoms and 3-4 and 5-7
25 double bond equivalents, respectively. The molecular formulas with the highest relative abundances in
26 Group III and IV contained 10-13 and 13-16 oxygen atoms and 7-9 and 9-11 double bond equivalents,
27 respectively. Observations of the oxygen content and the double bond equivalents of the SOA products
28 suggest a complex mixture of accretion reaction mechanisms, without an easily confirmable dominating
29 pathway.

30 **Keywords:** secondary organic aerosol; water-soluble organic compounds; HR-MS

31 **1. Introduction**

32 Atmospheric aerosols are strongly linked to adverse human health effects, visibility reduction and
33 climate change. Primary and secondary organic compounds constitute up to 90% of the aerosol mass
34 fraction (Kanakidou et al. 2005). Secondary organic aerosols (SOA) result from atmospheric oxidation
35 reactions of primary anthropogenic and biogenic compounds. Oxidation reactions increase organic
36 aerosol mass and lower the volatility of the gas phase compounds. Following this, SOA was thought to
37 result from gas phase reactions that yielded low volatility products (Kanakidou et al. 2005). However
38 SOA may also result from heterogeneous (Jang et al. 2001) and aqueous phase (Lim et al. 2005; Carlton
39 et al. 2007; Warren et al. 2009) reactions that result in an increase in the organic aerosol mass. It is likely
40 that a combination of homogeneous and heterogeneous reactions in various phases is responsible for
41 SOA production and evolution (Poschl 2005). The result is a complicated mixture of oxidized
42 carbonaceous compounds from both biogenic and anthropogenic sources. SOA contributes to negative
43 radiative forcing, but the magnitude of aerosol radiative forcing is highly uncertain (Fuzzi et al. 2006;
44 IPCC 2007). Observations of SOA in mass fractions higher than expected have been reported by Heald et
45 al. (2005) and Volkamer et al. (2006). A general “terpenoid character” in water-soluble aerosol organic
46 matter was reported from the molecular characterization observations of Schmitt-Kopplin et al. (2010),
47 further confirming the SOA dominance in aerosol. Atmospheric oxidation processes that contribute to
48 SOA occur at the molecular level, thus it is important to characterize the molecular aspects of various
49 types of SOA. These molecular aspects of laboratory generated SOA can then be compared to the
50 molecular aspects of ambient organic aerosol components.

51 The detailed analysis of the SOA products of α -pinene ozonolysis (Tolocka et al. 2004; Schrader et al.
52 2005; Tolocka et al. 2006; Heaton et al. 2007; Reinhardt et al. 2007; Heaton et al. 2009), limonene
53 ozonolysis (Walser et al. 2008; Bateman et al. 2009), and isoprene ozonolysis (Kroll et al. 2006; Surratt et

54 al. 2006; Nguyen et al. 2010) have been measured and characterized in previous research with a variety
55 of methods. Thus, it is well known that ozone reacts with α -pinene and other monoterpenes, forming
56 Criegee biradical intermediates and hydroxyl radicals (Atkinson et al. 1992; Schrader et al. 2005). Radical
57 chain propagation reactions produce organic peroxy radicals and alkoxy radicals which contribute to
58 SOA accretion products (Kroll and Seinfeld, 2008). Other first generation products may react by aldol
59 condensation, gem-diol formation, hemiacetal formation, organic peroxide formation and ester
60 condensation to form a variety of products (Gao et al. 2004; Tolocka et al. 2004; Bahreini et al. 2005;
61 Müller et al. 2008; Bateman et al. 2009; Yasmeen et al. 2010). Decomposition of accretion products may
62 occur as well (e.g. the cyclobutyl ring may open in the presence of a weak acid (Barsanti et al. 2006) or
63 organic peroxides may decompose to esters (Müller et al. 2008)) adding to the complex mixture of SOA
64 ozonolysis products collectively referred to as accretion products in this paper.

65 Electrospray ionization (ESI) coupled with FT-ICR MS provides detailed molecular characterization of
66 organic matter due to its extremely high resolution and mass accuracy (Marshall et al. 1998; Kujawinski
67 2002). FT-ICR MS offers up to 25 billion theoretical plates of separation (Hughey et al. 2002). The
68 ultrahigh-resolution of FT-ICR MS has revealed up to 63 individual masses within one nominal mass unit
69 (Grannas et al. 2006; Reemtsma 2009). Thus, it provides sufficiently accurate mass measurements for
70 the unequivocal assignment of molecular formulas containing C, H, and O up to 1000 u (Kim et al. 2006).
71 Ultrahigh-resolution and high-resolution mass spectrometry methods have been used for identification
72 of monoterpene SOA by other investigators (Reinhardt et al. 2007; Bateman et al. 2009; Heaton et al.
73 2009; Nguyen et al. 2010). In this paper, we present new complimentary results from FT-ICR MS analysis
74 of three α -pinene ozonolysis experiments with varied hydroxyl radical scavenging to examine the
75 resulting molecular composition of the experimental SOA. Analytical replicates were performed to
76 evaluate the technical reproducibility of the FT-ICR MS method used to identify the SOA components. A

77 full dataset of the identified molecular formulas for each of the experiments with averaged relative
78 abundances and absolute errors is provided in the associated supplemental information.

79 **2. Methods**

80 *2.1 α -pinene secondary organic aerosol experiments*

81 α -pinene SOA samples were generated in an isobaric Teflon bag chamber located at the US
82 Environmental Protection Agency in the Human Exposure and Atmospheric Sciences division. The
83 experimental variables were held constant except for the concentration of hexane (Table 1). Briefly,
84 ozone and α -pinene were reacted under dark conditions in a 9.0 m³ Teflon bag. The relative humidity in
85 the chamber was $\leq 4\%$ ($[\text{H}_2\text{O}] \leq 960$ ppmv). Seed aerosol was generated by aspirating dilute aqueous
86 solution of ammonium sulfate through a nebulizer jet (TSI Model 9050) and injecting the resulting
87 aerosol into the reaction chamber resulting in a concentration of < 0.1 microgram per cubic meter in the
88 chamber prior to hydrocarbon and ozone injections. A concentration of 0.7 ppmv of α -pinene and
89 hexane (at 0, 20, or 100 ppmv concentrations) were introduced into the chamber via a heated inlet.
90 Ozone was produced by passing 10 L/min of clean dry air through a UV ozone generator (model 1000
91 BT-12, Enaly Corporation, Shanghai, China). Ozone concentrations in the chamber were measured using
92 a TECO 49 photometric ozone monitor. Injection times, and ozone generator operations were identical
93 across the three experiments and resulted in maximum injected ozone concentrations observed = 250
94 ppbV in all three experiments. The exact amount of ozone introduced into the chamber is unknown,
95 because it began to react immediately, however ozone was generated only until it was detected at a
96 concentration of 250 ppbv. The reaction chamber was operated with a clean air make-up flow of 10
97 L/min to maintain positive pressure and constant chamber volume. The resulting SOA was collected at a
98 rate of 8 L/min for 22 hours on a pre-weighed Teflon impregnated glass fiber (TIGF) filter. A parallel
99 plate carbon strip denuder (Sunset Laboratory) was used to remove volatile species from the sampled

100 air. The 22 hour sampling period was used to maximize the aerosol collection for FT-ICR MS analysis,
101 however wall losses are expected to be enhanced during the extended periods. The actual wall losses
102 were not determined in these experiments. The TIGF filter was weighed for gravimetric determination of
103 the SOA mass. The filters were wrapped in aluminum foil and stored frozen.

104 *2.2 Sample preparation and ultrahigh-resolution FT-ICR MS analysis*

105 One quarter of the TIGF filter was removed with a stainless steel blade on a custom Teflon and stainless
106 steel apparatus. The filter pieces were weighed before and after cutting. The quarter sections were
107 extracted with 5 mL of a 50/50 mixture of acetonitrile (CH₃CN) (CHROMASOLVE for HPLC, Sigma Aldrich)
108 and water (CHROMASOLVE for HPLC, Sigma Aldrich) solution. The filters were extracted for 45 minutes
109 in a sonicating bath. Afterwards the solution was decanted and stored in a freezer until analysis.

110 The ultrahigh resolution mass spectrometric analysis was performed on a 7 T FT-ICR MS (LTQ FT Ultra,
111 Thermo Scientific) equipped with an ESI source. For the analysis, the signal was optimized with dilution
112 of CH₃CN/water (50/50) to 50%. The diluted solution was directly infused at 5 μLmin^{-1} into the ESI
113 interface. The ESI probe was placed in position "B" and the needle voltage was set between -3.7 and -3.8
114 kV (blanks were -4.0kV). Between samples the apparatus was flushed with a minimum of 500 μL of
115 CH₃CN/water (50/50), CH₃CN, and CH₃CN/water (50/50) until background noise levels were reached.
116 Negative ion mass spectra were collected using full scan analysis ($100 < m/z < 1000$). The mass resolving
117 power was set at 400,000. Automatic gain control was used to consistently fill the instrument with the
118 same number of ions ($n = 1 \times 10^6$) for each acquisition and to avoid space charge effects from over filling
119 the mass analyzer. The instrument was externally calibrated in negative ion mode with a standard
120 solution of sodium dodecyl sulfate and taurocholic acid, and the resulting mass accuracy was better than
121 2 ppm. More than 200 individual mass spectra were collected and stored as transients by use of Thermo
122 Xcalibur software. Replicate full scans were collected for two samples. Variances in the relative

123 abundances and reproducibility of low relative abundance signals were calculated from the replicate
124 analyses. Chamber blank filter samples were treated in the same way, but no replicate analyses were
125 performed.

126 *2.3 Data processing and chemical formula assignments*

127 Approximately 200 transients recorded in the time domain were co-added with Sierra Analytics
128 Composer software (Mazzoleni et al. 2010). Co-addition of time domain data prior to Fourier
129 transformation enhances the analyte signal-to-noise ratio (Kujawinski et al. 2002; Stenson et al. 2003).
130 Internal recalibration of the mass spectra (Sleighter et al. 2008; Mazzoleni et al. 2010) was done using
131 three homologous series defined by oxygen content of 4, 8, and 12 and double bond equivalents (DBE)
132 of 3, 5, and 7 (see also Table S-1). The formula calculator, based on the PREDATOR algorithm², uses a
133 Kendrick mass analysis (Hughey et al. 2001) to sort ions into CH₂ homologous series and then assigns the
134 *de novo* molecular formulas. Molecular formulas were determined for ions with relative abundances >
135 0.1% in the range of 100 < m/z < 850. The formula calculator was set to allow up to 100 carbon, 200
136 hydrogen, and 20 oxygen atoms per elemental composition. Additional molecular formula calculations
137 were performed to include up to 3 nitrogen atoms and a *de novo* cutoff of 500 u. The relative
138 abundance threshold of 0.1% (a software minimum) was 20-25 times higher than the root mean square
139 of the noise values between 900 < m/z < 1000 of the SOA mass spectra. The threshold values for blanks
140 ranged from 0.15 to 0.29% and were 6 times the root mean square values between 900 < m/z < 1000.

141 Data filtering of the assigned formulas was done by applying rules and assumptions as described by Koch
142 et al. (2005). Further description is available in the corresponding supporting information. Additionally,
143 molecular formulas resulting in measurement errors > 3 ppm were discarded. After preliminary data
144 filtering, the samples were aligned into a unified list of molecular formulas. The alignment facilitates
145 comparisons for FT-ICR MS replicate analysis, experimental SOA and literature data. Replicate analyses

146 were used to evaluate the technical reproducibility of analytical method. The absolute measurement
147 errors and relative abundances for replicate formulas were averaged and the standard deviations were
148 calculated.

149 **3. Results and discussion**

150 *3.1 Chemical formula assignments and homologous series*

151 More than 900 monoisotopic compounds containing C, H, and O were identified from the negative
152 electrospray ultrahigh resolution FT-ICR mass spectra of α -pinene ozonolysis SOA. Molecular formulas
153 with naturally abundant carbon-13 were identified and they corresponded to 99% of the monoisotopic
154 compounds. The high number of corresponding isotopic molecular formulas confirms the single charge
155 state and analyte detection and identification. The majority of negative ions were consistently detected
156 in all of the samples. The overall technical reproducibility of the FT-ICR MS method was determined to
157 be 77% from replicate analysis of AP-SOA-20H and AP-SOA-100H. An average relative abundance and
158 error were calculated for the replicated samples. Overall between the three samples, 664 analytes were
159 found in all three SOA samples, 218 analytes were in two of the three samples and 39 were unique. 36
160 unique analytes appeared in AP-SOA-0H and 202 analytes were unique to the hexane experiments, AP-
161 SOA-20H and AP-SOA-100H. The chemical characterization of the SOA components is presented below
162 and the differences between the three experimental conditions are discussed.

163 The homologous series of α -pinene SOA analytes are shown in Figure 1. Using semi-transparent primary
164 colors for each experiment, the unique and common formulas for the experiments are shown
165 simultaneously. Overall, the identified molecular formulas appear to be consistent between the three
166 experiments with variable concentrations of hexane (Figure 1A). Typically, the unique formulas appear
167 at the lowest and highest members of the homologous series. A few unique homologous series were
168 observed in the dataset corresponding to AP-SOA-100H. Common analytes between any two

169 experiments were observed (green, orange and purple symbols). To further evaluate the commonalities,
170 a variation of the Kendrick plot is shown in Figure 1B. The relative abundance is represented with the
171 symbol size. Thus, the largest symbols correspond to the most intense masses in the mass spectra. The
172 base peak, m/z 185, corresponds to the large symbol with Kendrick mass defect 0.125. In this figure with
173 the scaled symbols, the unique formulas in the homologous series appear to be less significant. Relative
174 significance in this sense is based on the assumption that members of a homologous series would not
175 have highly variable electrospray ionization efficiencies.

176 Consistent with the previous analyses of monoterpene SOA (Tolocka et al. 2004; Reinhardt et al. 2007),
177 the ESI mass spectra appears to contain distinct groups of ions (Figure 2). They are often referred to as
178 monomers, dimers, trimers and tetramers (Tolocka et al. 2004), reflecting a widely-held presumption
179 that the accretions occur predominantly between first generation SOA products such that a basic
180 “terpenoid” structure is retained. Because there is evidence of multiple accretions involving the Criegee
181 intermediates, hydroperoxides and terpenoid degradation products that do not necessarily retain the
182 terpenoid structure, we refer to these mass ranges as Group I, Group II, Group III and Group IV. They are
183 defined as follows: Group I is $100 < m/z < 300$; Group II is $300 < m/z < 475$; Group III is $475 < m/z < 650$;
184 and Group IV is $650 < m/z < 850$. The total relative abundance for each group decreases with increasing
185 mass. The groups are also apparent in Figure 1B. However, we observe some homologous series which
186 span over more than one group. The consistent presence of low relative abundance analytes between
187 the traditional high relative abundance groups demonstrates a variety of degradation and accretion of
188 the basic “terpenoid” unit.

189 Hydroxyl radicals are produced during ozonolysis reactions at a high rate (0.7-0.85 molar ratio (Schrader
190 et al. 2005; Atkinson et al. 1992). Hydroxyl radicals affect SOA composition by reacting via hydrogen
191 atom abstraction and addition across double bonds. As a result, hydroxyl radicals increase the amount

192 of oxygen in the secondary products, as well as fracture the carbon skeleton into more volatile low
193 molecular weight analytes ($m/z < 300$). In this work, we observed a higher O:C ratio of AP-SOA-0H SOA
194 compared to the other experiments. Likewise, in the SOA produced without hexane, unique compounds
195 appeared in the low end of the homologous series, whereas in SOA produced with hexane, unique
196 compounds appear at the high end of homologous series. Furthermore, the production efficiency of ions
197 m/z 357, 367 and 539 in Groups II and III sharply increased with the presence of hexane. The relative
198 abundance of several group I ions decreased in the presence of hexane. They were m/z 185, 199, 215,
199 231 and 261. Iinuma et al. (2005) notes the disappearance of 185 (hydroxypinonaldehyde), 215 and 231
200 for higher concentrations of scavenger. The trend is further confirmed by the distribution of signal
201 intensity for the groups. Group I represented 37% of the total signal intensity for AP-SOA-0H, compared
202 to 26% and 30% for AP-SOA-20H and AP-SOA-100H. Because a greater fraction of the signal intensity is
203 in groups II and III for experiments with hexane, scavenging of hydroxyl radicals may produce less
204 volatile SOA products and enhance particle formation by accretions involving the stabilized Criegee
205 intermediate derived alkylperoxy radical.

206 *3.2 Carbon number trends*

207 Trends with respect to the number of carbon atoms in the identified molecular formulas were explored.
208 Because of the consistency between experiments with a few exceptions, an average relative abundance
209 was calculated for each molecular formula of the three α -pinene ozonolysis experiments. DBE were
210 plotted as a function of carbon number (Figure 3A; Table 2). Similar to earlier observations of α -pinene
211 ozonolysis SOA (Tolocka et al. 2004), we observed clusters of peaks at mass ranges with approximately
212 10, 20, 30, and 40 carbon atoms (Figure 3). In Group I, SOA analytes had formula derived DBE values of 2
213 – 6 with 5 – 17 carbon atoms. The most abundant species, including the base peak m/z 185 (pinic acid),
214 were 8 – 11 carbon atoms with DBE values of 3 and 4. These compounds appear to be similar to the

215 precursor compound, α -pinene and are characterized by the oxidation of two side chains with the
216 cyclobutyl ring as a basic structural element (Bahreini et al. 2005). This general structure has been
217 confirmed by investigations of some prominent group I molecules by fragmentation and LC-NMR-MS
218 (Schrader et al. 2005). Beyond the peak intensities, evidence for considerable oxidation of the Group I
219 analytes was found by inspection of the number of oxygen atoms (Figure 3B; Table 2). The range of
220 oxygen atoms was 3 – 9, with peak abundances at 3 – 6. The high number of oxygen atoms in the Group
221 I analytes is very likely a result of radical reactions that enhance hydrogen abstraction in the presence of
222 molecular oxygen. Another possible explanation is that low molecular weight accretion reactions play a
223 substantial role in increasing the oxygen content.

224 The range of DBE values for the Group II analytes was 2 – 9 with a range of 12 – 27 carbon atoms. The
225 most abundant species in the group were 17 – 20 carbon atoms with DBE values 5 and 6. These high
226 abundance compounds have been a primary focus of several studies (Tolocka et al. 2004; Tolocka et al.
227 2006; Heaton et al. 2007; Yasmeen et al. 2010). The compounds with DBE 5 and 6 are formed by
228 accretion reactions that retain a majority of the monoterpene carbon skeleton, thus they are often
229 referred to as dimers. The accretion reactions proceed via a combination of Criegee radical, organic
230 peroxides and their degradation products, hemiacetal reactions, aldol condensation, and ester
231 condensation reactions. Reaction mechanisms cannot be well distinguished, because condensation
232 reaction products produce compounds with DBE 5 and 6 with and without acid catalysis. For example,
233 Yasmeen et al. (2010) discussed the formation of the m/z 357 with DBE 5 from cis-pinic acid and
234 diaterpenylic acid after an esterification. Overall, Group II analytes had a broad range of oxygen atoms
235 (4 – 13) in the assigned molecular formulas, as expected from the high degree of complexity observed in
236 the mass spectra for this region. Criegee radical reactions with Group I products (Bateman et al. 2009)
237 provide a plausible link between the compounds with high intensities of the Group I analytes and the

238 high intensities of Group II analytes. However, the link between Group II and Group III analytes is less
239 clear.

240 Overall the Group III analytes have a range of DBE values from 5 – 11 and carbon atoms from 20 – 36.
241 The highest intensity compounds in the group have 26 – 28 carbon atoms and DBE values of 7 – 8. These
242 Group III compounds may represent a DBE increase of 2 or 3 from the Group II compounds with DBE 5
243 and 6. However the wide number of compounds with vastly different carbon numbers but similar DBE
244 values, suggests a wide number of accretion reaction pathways. The oxygen content of Group III
245 analytes ranges from 7 – 16 atoms, with the high intensity compounds containing between 9 – 12
246 oxygen atoms. Analytes in Group IV had DBE values from 7 – 11 with 30 – 41 carbon atoms. The most
247 prominent analytes had 34 – 38 carbons and DBE's between 9 and 11. The oxygen content spanned 11 –
248 18 oxygen atoms and the high peak intensity compounds between 12 and 16 atoms. In general, O:C
249 decreases with increasing molecular weight. It was suggested (Reinhardt et al. 2007) that this decreased
250 mass contribution of oxygen indicates a dominance of dehydration reaction pathways like aldol and
251 ester condensation. However, we did not observe a decrease in the H:C ratio with increasing molecular
252 weight to confirm the loss of water. Instead radical reactions involving the Criegee intermediate and/or
253 organic peroxy radicals which eliminate oxygen (Keywood et al. 2004; Docherty et al 2005; Kroll and
254 Seinfeld, 2008) may explain the observed trends.

255 *3.3 Elemental ratios and the van Krevelen diagram*

256 Elemental ratios of hydrogen and oxygen relative to carbon are useful for classification of complex
257 organic matter. The van Krevelen diagram, a plot of H:C vs. O:C, for α -pinene SOA is shown in Figure 4A.
258 Consistent with Figures 2 and 3, the data shown in this plot are from the complete dataset with an
259 averaged relative abundance from the three experiments. This plot indicates that a majority of the
260 medium to high abundance compounds have H:C ratios of 1.4 to 1.6 and O:C ratios of 0.30 – 0.70. Group

261 I analytes have the widest ranges of elemental ratios (Table 2). The ranges of the O:C and H:C values
262 decreased with increasing molecular weight (Figure 4). The mean values of O:C for each group were
263 0.55, 0.46, 0.43 and 0.42. The median values were slightly lower (0.54, 0.45, 0.42 and 0.42) but also
264 consistently decreased from Group I to Group IV. Both the mean and median H:C values were all
265 approximately 1.5, despite the decreasing range of H:C from Group I to Group IV. The H:C values
266 indicate the identified SOA compounds are aliphatic and alicyclic. When compared with the H:C ratio of
267 α -pinene (1.6), the average H:C value of the SOA indicates some hydrogen loss, likely due to H atom
268 abstractions, dehydration, and acidification. In this work using negative mode ESI analysis, we did not
269 observe aromatic structures in the SOA compounds as were reported previously (Bateman et al. 2009;
270 Heaton et al. 2009). Consistent with the Kendrick plot (Figure 1), a number of homologous series were
271 observed in the van Krevelen diagram shown in Figure 4A. The homologous series appear as diagonal
272 lines originating from the top left corner of the diagram. Note, the points on the van Krevelen diagram
273 overlap. Isoabundance contour plots provide a visual aid for the interpretation of the density of points
274 and their relative abundance in the van Krevelen space. For example, following the peak abundances in
275 the plot, two prominent slopes are observed at -1 and -0.7. These slopes are similar to those observed in
276 ambient aerosol mass spectrometry measurements (Heald et al. 2010; Ng et al. 2011).

277 *3.4 Carbon oxidation states of α -pinene SOA*

278 As proposed by Kroll et al. (2011), the oxidation state of carbon (OS_c) can be estimated from the
279 elemental ratios given by: $OS_c \approx 2(O:C) - H:C$. Aerosol volatility is positively correlated to the average
280 oxidation state (Hao et al. 2011). Thus, estimation of the oxidation state provides insight for the
281 volatility of the SOA analytes. The 922 compounds were represented by 192 OS_c values (Figure 5A).
282 Similar to the carbon number trends plots in Figure 3, four groups of compounds appeared. Consistent
283 with decreasing O:C range with increasing molecular weight (Group I – Group IV) we observed a

284 decreasing range of OS_c values. The decreasing group mean values are -0.42, -0.58, -0.64 and -0.68 for
285 Group I – Group IV, respectively (Table 2). The isoabundance plot illustrates the decreasing range in the
286 OS_c values with increasing mass, but similar OS_c values for the peak intensities of the groups. The range
287 of OS_c values for the peak intensities of each group decreases with increasing molecular weight. Group I
288 ranged from -0.20 to -1.0, Group II ranged from -0.33 to -0.95, Group III ranged from -0.59 to -0.80 and
289 Group IV ranged from -0.63 to -0.82. The overall relative abundance weighted average OS_c was -0.63.
290 This value intersects the peak intensity values of OS_c for each group, despite the wide ranges and
291 decreasing group mean values. Furthermore, this value is similar to other OS_c values determined from
292 elemental observations of SOA (Bateman et al. 2009; Shilling et al. 2009; Chhabra et al. 2010; Kroll et al.
293 2011).

294 **3.5 Relative abundance weighted bulk values**

295 Relative abundance weighted ratios were determined using a method previously described for isoprene
296 ozonolysis SOA (Nguyen et al. 2010) and limonene ozonolysis SOA (Bateman et al. 2009). Relative
297 abundance weighting assumes that the signal intensity corresponds linearly with the analyte
298 concentration. Thus, it neglects the differences in the molecular ESI efficiencies which vary with
299 molecular weight and structure. This assumption is viable because the observed functional groups and
300 overall structural character of α -pinene SOA is presumably similar, thus the molecules are not expected
301 to have highly variable ESI efficiencies. The actual ESI efficiencies are not known. The relative abundance
302 weighted ratios facilitate bulk characterization of the SOA samples to literature values (Table 3). The
303 relative abundance weighted O:C values ($O:C_w$) of α -pinene (0.43 ± 0.03 to 0.46 ± 0.02) and limonene
304 SOA (0.45 ± 0.09) (Bateman et al. 2009) indicate an overall lower extent of oxidation compared to
305 isoprene SOA (0.63 ± 0.26) (Nguyen et al. 2010). This may be attributed to the ring opening that occurs
306 with ozonolysis of the 10 carbon atom monoterpene which retains most of the molecule as an intact

307 carbon chain. Instead, ozonolysis of isoprene cleaves the 5 carbon atom chain, yielding two small
308 oxygenated molecules that participate in secondary accretion reactions. The accretion of small
309 molecules described in SOA formation during isoprene ozonolysis (Nguyen et al. 2010) suggests that
310 some smaller oxygenated products of α -pinene ozonolysis may also undergo accretion reactions in a
311 similar manner. Minor differences were observed in the relative abundance weighted bulk properties
312 between α -pinene SOA formed in the presence of hexane (AP-SOA-20H and AP-SOA-100H) and without
313 hexane (AP-SOA-0H). Most notably, AP-SOA-0H had an O:C_w ratio of 0.46 ± 0.02 compared to AP-SOA-
314 20H and 100H O:C_w values of 0.44 ± 0.03 and 0.44 ± 0.02 . Although minor, this difference may reflect
315 the overall higher oxidation potential in conditions with higher hydroxyl radical concentrations.
316 Likewise, a slightly higher relative abundance weighted OM:OC ratio was observed for the AP-SOA-0H
317 sample than the experiments with hexane. The relative abundance weighted H:C ratios were similar
318 over all of the experiments.

319 ***3.6 Comparison of limonene ozonolysis SOA and α -pinene ozonolysis SOA***

320 A complex array of SOA products are expected from monoterpene ozonolysis. However, some
321 similarities might be expected in the SOA from the ozonolysis of different monoterpene precursors. To
322 evaluate this, we compared the identified molecular formulas of α -pinene SOA (n = 922) in this work to
323 the identified molecular formulas of limonene SOA (n = 903) from Bateman et al. (2009). The precursor
324 molecules have the same number of carbon atoms and DBE, but α -pinene has a bicyclic structure with
325 one double bond and limonene has a monocyclic structure with two double bonds. Additionally, the SOA
326 was generated without use of seed aerosol in the limonene ozonolysis experiments. Despite these
327 differences, the weighted ratios of O:C_w, H:C_w and OM:OC_w were not significantly different and 63% of
328 the α -pinene SOA molecular formulas were identical to the limonene SOA molecular formulas. Note:
329 molecular formulas may represent several different isomers and do not provide structural information.

330 However, the presence of higher DBE compounds in the limonene SOA were unique and a greater range
331 of O:C ratios were found in the α -pinene SOA. The highest levels of O:C were found Group I compounds.
332 Another interesting difference between the two datasets is the consistency of the DBE differences
333 between the groups. The limonene SOA appears to have a consistent DBE increase of 2, while α -pinene
334 SOA appear to have DBE increases of 2 and 3. This indicates additional accretion reaction pathways for
335 the α -pinene intermediates.

336 **4. Summary and Conclusions**

337 The molecular composition of three α -pinene ozonolysis experiments with variable amounts of hexane
338 was investigated. Minor differences in the SOA composition between the experiments were observed.
339 They include differences in the homologous series and in the ion intensities of a few specific
340 compounds. This may correspond to an increase in higher molecular weight compounds with hexane.
341 Thus, the hydroxyl radical scavenger concentration partially suppresses the hydroxyl radical reactions,
342 reducing HO₂ and allowing a greater number of alkylperoxy accretions to proceed, thus having a minor
343 effect upon the SOA composition. Group specific characterization of the SOA showed that the O:C values
344 decreased as molecular weight increased (0.55 in Group I – 0.42 in Group IV). Likewise, the ranges of O:C
345 values decreased from Group I to Group IV. This is an indication of accretion reactions that eliminate
346 oxygen in the form of water, peroxide or other small oxygenated molecules. The relative abundance
347 weighted O:C and OM:OC values for α -pinene and limonene SOA samples were similar, but less than
348 isoprene SOA. As expected, 63% of the molecular formulas identified in α -pinene SOA were identical to
349 those identified in limonene SOA. Evaluation of the homologous series, range of carbon numbers, DBE
350 values and the range of oxygen numbers in the molecular formulas in each group indicates a variety of
351 complex accretion reactions without uniform oligomerization patterns. The accretion reactions may

352 involve a wide number of combinations of terpenoids, Criegee bi-radical intermediates, hydroperoxides
353 and degradation products.

354 **Acknowledgements**

355 Financial support for this research was provided by a research seed grant from the Michigan Tech
356 Research for Excellence Fund and the Los Alamos National Laboratory–Laboratory Directed Research
357 and Development program. We thank Drs. Melissa Soule & Elizabeth Kujawinski of the Woods Hole
358 Oceanographic Institution (WHOI) Mass Spectrometry Facility for instrument time and data acquisition
359 assistance. The facility is supported by NSF OCE-0619608 and the Gordon and Betty Moore Foundation.
360 A. L. Putman thanks the WHOI Mass Spectrometry Facility for a travel fellowship. S. Kundu thanks David
361 J. Pruetz and Valeria L. Pruetz for fellowship support via the Department of Chemistry at Michigan Tech.
362 We thank the anonymous reviewers who provided helpful suggestions to improve the manuscript. The
363 U.S. Environmental Protection Agency through its Office of Research and Development collaborated in
364 the research described here. The manuscript has been subjected to external peer review and has been
365 cleared for publication. Mention of trade names or commercial products does not constitute an
366 endorsement or recommendation for use.

367 **Supporting Information**

368 A compact list of all assigned molecular formulas, DBE values, MS relative abundances, and assignment
369 errors for each sample is provided. Additional figures for data visualization are also provided. Additional
370 data may be provided upon request

371 **References**

- 372 Atkinson, R., S. M. Aschmann, J. Arey, and B. Shorees (1992). "Formation of OH Radicals in the Gas-
 373 Phase Reactions of O₃ with a Series of Terpenes". *Journal of Geophysical Research-Atmospheres*,
 374 97(D5): 6065-6073.
- 375 Bahreini, R., M. D. Keywood, N. L. Ng, V. Varutbangkul, S. Gao, R. C. Flagan, J. H. Seinfeld, D. R. Worsnop
 376 and J. L. Jimenez (2005). "Measurements of secondary organic aerosol from oxidation of
 377 cycloalkenes, terpenes, and m-xylene using an Aerodyne aerosol mass spectrometer."
 378 *Environmental Science and Technology* **39**(15): 5674-88.
- 379 Barsanti, K. C. and J. F. Pankow (2006). "Thermodynamics of the formation of atmospheric organic
 380 particulate matter by accretion reactions - Part 3: Carboxylic and dicarboxylic acids."
 381 *Atmospheric Environment* **40**(34): 6676-6686.
- 382 Bateman, A. P., S. A. Nizkorodov, J. Laskin and A. Laskin (2009). "Time-resolved molecular
 383 characterization of limonene/ozone aerosol using high-resolution electrospray ionization mass
 384 spectrometry." *Physical Chemistry Chemical Physics* **11**(36): 7931-7942.
- 385 Carlton, A. G., B. J. Turpin, K. E. Altieri, S. Seitzinger, A. Reff, H. J. Lim and B. Ervens (2007). "Atmospheric
 386 oxalic acid and SOA production from glyoxal: Results of aqueous photooxidation experiments."
 387 *Atmospheric Environment* **41**(35): 7588-7602.
- 388 Chhabra, P. S., R. C. Flagan and J. H. Seinfeld (2010). "Elemental analysis of chamber organic aerosol
 389 using an aerodyne high-resolution aerosol mass spectrometer." *Atmospheric Chemistry and
 390 Physics* **10**(9): 4111-4131.
- 391 Docherty, K.S. and Ziemann, P.J. (2003). "Effects of stabilized Criegee intermediate and OH radical
 392 scavengers on aerosol formation from reactions of β-pinene with O³". *Aerosol Science and
 393 Technology*, **37**(11): 877-891.
- 394 Fuzzi, S., et al. (2006). "Critical assessment of the current state of scientific knowledge, terminology, and
 395 research needs concerning the role of organic aerosols in the atmosphere, climate, and global
 396 change." *Atmospheric Chemistry and Physics* **6**: 2017-2038.
- 397 Gao, S., M. Keywood, N. L. Ng, J. Surratt, V. Varutbangkul, R. Bahreini, R. C. Flagan and J. H. Seinfeld
 398 (2004). "Low-molecular-weight and oligomeric components in secondary organic aerosol from
 399 the ozonolysis of cycloalkenes and alpha-pinene." *Journal of Physical Chemistry A* **108**(46):
 400 10147-10164.
- 401 Grannas, A. M., W. C. Hockaday, P. G. Hatcher, L. G. Thompson and E. Mosley-Thompson (2006). "New
 402 revelations on the nature of organic matter in ice cores." *Journal of Geophysical Research-
 403 Atmospheres* **111**(D4).
- 404 Hao, L. Q., et al. (2011). "Mass yields of secondary organic aerosols from the oxidation of α-pinene
 405 and real plant emissions." *Atmospheric Chemistry and Physics* **11**(4): 1367-1378.
- 406 Heald, C. L., D. J. Jacob, R. J. Park, L. M. Russell, B. J. Huebert, J. H. Seinfeld, H. Liao and R. J. Weber
 407 (2005). "A large organic aerosol source in the free troposphere missing from current models."
 408 *Geophysical Research Letters* **32**(18).
- 409 Heald, C. L., et al. (2010). "A simplified description of the evolution of organic aerosol composition in the
 410 atmosphere." *Geophysical Research Letters* **37**: -.
- 411 Heaton, K. J., M. A. Dreyfus, S. Wang and M. V. Johnston (2007). "Oligomers in the early stage of
 412 biogenic secondary organic aerosol formation and growth." *Environmental Science and
 413 Technology* **41**(17): 6129-36.
- 414 Heaton, K. J., R. L. Sleigher, P. G. Hatcher, W. A. t. Hall and M. V. Johnston (2009). "Composition
 415 domains in monoterpene secondary organic aerosol." *Environmental Science and Technology*
 416 **43**(20): 7797-802.

417 Hughey, C. A., C. L. Hendrickson, R. P. Rodgers, A. G. Marshall and K. N. Qian (2001). "Kendrick mass
418 defect spectrum: A compact visual analysis for ultrahigh-resolution broadband mass spectra."
419 *Analytical Chemistry* **73**(19): 4676-4681.

420 Hughey, C. A., R. P. Rodgers and A. G. Marshall (2002). "Resolution of 11 000 compositionally distinct
421 components in a single Electrospray ionization Fourier transform ion cyclotron resonance mass
422 spectrum of crude oil." *Analytical Chemistry* **74**(16): 4145-4149.

423 Iinuma, Y., O. Böge, Y. K. Miao, B. Sierau, T. Gnauk, H. Herrmann (2005). "Laboratory studies on
424 secondary organic aerosol formation from terpenes." *Faraday Discussions* **130**: 279-294.

425 IPCC (2007). *Climate Change 2007: Synthesis Report*. Contribution of working groups I, II, III to the
426 Fourth Assessment Report of the Intergovernmental Panel on Climate Change. P. Core Writing
427 Team, R.K., Reisinger, A. Geneva, Switzerland, IPCC: 1-104.

428 Jang, M. and R. M. Kamens (2001). "Atmospheric secondary aerosol formation by heterogeneous
429 reactions of aldehydes in the presence of a sulfuric acid aerosol catalyst." *Environmental Science
430 and Technology* **35**(24): 4758-4766.

431 Kanakidou, M., et al. (2005). "Organic aerosol and global climate modelling: a review." *Atmospheric
432 Chemistry and Physics* **5**: 1053-1123.

433 Keywood, M.D., J. H. Kroll, V. Varutbangkul, R. Bahreini, R. C. Flagan, R.C. and J. H. Seinfeld (2004).
434 "Secondary organic aerosol formation from cyclohexene ozonolysis: Effect of OH scavenger and
435 the role of radical chemistry". *Environmental Science & Technology*, **38**(12): 3343-3350.

436 Kim, S., R. P. Rodgers and A. G. Marshall (2006). "Truly "exact" mass: Elemental composition can be
437 determined uniquely from molecular mass measurement at similar to 0.1 mDa accuracy for
438 molecules up to similar to 500 Da." *International Journal of Mass Spectrometry* **251**(2-3): 260-
439 265.

440 Koch, B. P., M. R. Witt, R. Engbrodt, T. Dittmar and G. Kattner (2005). "Molecular formulae of marine
441 and terrigenous dissolved organic matter detected by electrospray ionization Fourier transform
442 ion cyclotron resonance mass spectrometry." *Geochimica et Cosmochimica Acta* **69**(13): 3299-
443 3308.

444 Kroll, J. H., et al. (2011). "Carbon oxidation state as a metric for describing the chemistry of atmospheric
445 organic aerosol." *Nature Chemistry* **3**(2): 133-9.

446 Kroll, J. H., N. L. Ng, S. M. Murphy, R. C. Flagan and J. H. Seinfeld (2006). "Secondary organic aerosol
447 formation from isoprene photooxidation." *Environmental Science and Technology* **40**(6): 1869-
448 1877.

449 Kroll, J. H. and J. H. Seinfeld (2008). "Chemistry of secondary organic aerosol: Formation and evolution of
450 low-volatility organics in the atmosphere." *Atmospheric Environment* **42**: 3593-3624.

451 Kujawinski, E. B. (2002). "Electrospray ionization Fourier transform ion cyclotron resonance mass
452 spectrometry (ESI FT-ICR MS): characterization of complex environmental mixtures."
453 *Environmental Forensics* **3**(3-4): 207-216.

454 Kujawinski, E. B., P. G. Hatcher and M. A. Freitas (2002). "High-resolution Fourier transform ion cyclotron
455 resonance mass spectrometry of humic and fulvic acids: Improvements and comparisons."
456 *Analytical Chemistry* **74**(2): 413-419.

457 Lim, H. J., A. G. Carlton and B. J. Turpin (2005). "Isoprene forms secondary organic aerosol through cloud
458 processing: Model simulations." *Environmental Science and Technology* **39**(12): 4441-4446.

459 Marshall, A. G., C. L. Hendrickson and G. S. Jackson (1998). "Fourier Transform Ion Cyclotron Resonance
460 Mass Spectrometry: A Primer." *Mass Spectrometry Reviews* **17**: 1-17.

461 Mazzoleni, L. R., B. M. Ehrmann, X. H. Shen, A. G. Marshall and J. L. Collett (2010). "Water-Soluble
462 Atmospheric Organic Matter in Fog: Exact Masses and Chemical Formula Identification by
463 Ultrahigh-Resolution Fourier Transform Ion Cyclotron Resonance Mass Spectrometry."
464 *Environmental Science and Technology* **44**(10): 3690-3697.

465 Müller, L., M. C. Reinnig, J. Warnke and T. Hoffmann (2008). "Unambiguous identification of esters as
466 oligomers in secondary organic aerosol formed from cyclohexene and cyclohexene/ α -pinene
467 ozonolysis." *Atmospheric Chemistry and Physics* **8**(5): 1423-1433.

468 Ng, N.L., M. R. Canagaratna, J. L. Jimenez, P. S. Chhabra, J. H. Seinfeld and D. R. Worsnop (2011)
469 "Changes in organic aerosol composition with aging inferred from aerosol mass spectra."
470 *Atmospheric Chemistry and Physics* **11**, 6465-6474.

471 Nguyen, T. B., A. P. Bateman, D. L. Bones, S. A. Nizkorodov, J. Laskin and A. Laskin (2010). "High-
472 resolution mass spectrometry analysis of secondary organic aerosol generated by ozonolysis of
473 isoprene." *Atmospheric Environment* **44**(8): 1032-1042.

474 Poschl, U. (2005). "Atmospheric aerosols: Composition, transformation, climate and health effects."
475 *Angewandte Chemie-International Edition* **44**(46): 7520-7540.

476 Reemtsma, T. (2009). "Determination of molecular formulas of natural organic matter molecules by
477 (ultra-) high-resolution mass spectrometry Status and needs." *Journal of Chromatography A*
478 **1216**(18): 3687-3701.

479 Reinhardt, A., C. Emmenegger, B. Gerrits, C. Panse, J. Dommen, U. Baltensperger, R. Zenobi and M.
480 Kalberer (2007). "Ultrahigh mass resolution and accurate mass measurements as a tool to
481 characterize oligomers in secondary organic aerosols." *Analytical Chemistry* **79**(11): 4074-4082.

482 Schmitt-Kopplin, P., A. Gelencser, E. Dabek-Zlotorzynska, G. Kiss, N. Hertkorn, M. Harir, Y. Hong and I.
483 Gebefugi (2010). "Analysis of the unresolved organic fraction in atmospheric aerosols with
484 ultrahigh-resolution mass spectrometry and nuclear magnetic resonance spectroscopy:
485 organosulfates as photochemical smog constituents." *Analytical Chemistry* **82**(19): 8017-26.

486 Schrader, W., J. Geiger and M. Godejohann (2005). "Studies of complex reactions using modern
487 hyphenated methods: α -Pinene ozonolysis as a model reaction." *Journal of Chromatography*
488 **A 1075**(1-2): 185-196.

489 Shilling, J. E., et al. (2009). "Loading-dependent elemental composition of α -pinene SOA particles."
490 *Atmospheric Chemistry and Physics* **9**(3): 771-782.

491 Sleighter, R. L., G. A. McKee, Z. Liu and P. G. Hatcher (2008). "Naturally present fatty acids as internal
492 calibrants for Fourier transform mass spectra of dissolved organic matter." *Limnology and*
493 *Oceanography-Methods* **6**: 246-253.

494 Stenson, A. C., A. G. Marshall and W. T. Cooper (2003). "Exact masses and chemical formulas of
495 individual Suwannee River fulvic acids from ultrahigh resolution electrospray ionization Fourier
496 transform ion cyclotron resonance mass spectra." *Analytical Chemistry* **75**(6): 1275-1284.

497 Surratt, J. D., et al. (2006). "Chemical composition of secondary organic aerosol formed from the
498 photooxidation of isoprene." *Journal of Physical Chemistry A* **110**(31): 9665-9690.

499 Tolocka, M. P., K. J. Heaton, M. A. Dreyfus, S. Wang, C. A. Zordan, T. D. Saul and M. V. Johnston (2006).
500 "Chemistry of particle inception and growth during α -pinene ozonolysis." *Environmental*
501 *Science and Technology* **40**(6): 1843-1848.

502 Tolocka, M. P., M. Jang, J. M. Ginter, F. J. Cox, R. M. Kamens and M. V. Johnston (2004). "Formation of
503 oligomers in secondary organic aerosol." *Environmental Science and Technology* **38**(5): 1428-
504 1434.

505 Volkamer, R., J. L. Jimenez, F. San Martini, K. Dzepina, Q. Zhang, D. Salcedo, L. T. Molina, D. R. Worsnop
506 and M. J. Molina (2006). "Secondary organic aerosol formation from anthropogenic air pollution:
507 Rapid and higher than expected." *Geophysical Research Letters* **33**(17).

508 Walser, M. L., Y. Desyaterik, J. Laskin, A. Laskin and S. A. Nizkorodov (2008). "High-resolution mass
509 spectrometric analysis of secondary organic aerosol produced by ozonation of limonene."
510 *Physical Chemistry Chemical Physics* **10**(7): 1009-22.

511 Warren, B., Q. G. J. Malloy, L. D. Yee and D. R. Cocker (2009). "Secondary organic aerosol formation from
512 cyclohexene ozonolysis in the presence of water vapor and dissolved salts." *Atmospheric*
513 *Environment* **43**(10): 1789-1795.

514 Yasmeen, F., R. Vermeylen, R. Szmigielski, Y. Iinuma, O. Böge, H. Herrmann, W. Maenhaut and M. Claeys
515 (2010). "Terpenylic acid and related compounds: precursors for dimers in secondary organic
516 aerosol from the ozonolysis of alpha- and beta-pinene." *Atmospheric Chemistry and Physics*
517 **10**(19): 9383-9392.

518

519

520 **Tables**521 **Table 1: A complete list of the samples with the extraction data**

Sample ID*	Hexane Concentration (ppmv)	Mass of aerosol collected (mg)	Weight percent extracted (%)	Mass of aerosol extracted (mg)	Concentration for ESI-MS analysis (ng/ μ L)
AP-SOA-0H	0	2.6783	24.7	0.6615	66.2
AP-SOA-20H	20	3.1740	27.7	0.8792	87.9
AP-SOA-100H	100	2.1657	24.9	0.6042	60.4
AP-SOA-0H-B	n/a	0	25.5	0	0
AP-SOA-20H-B	n/a	0	24.6	0	0
AP-SOA-100H-B	n/a	0	26.1	0	0

522 *Sample names were constructed to indicate α -pinene SOA (AP-SOA), the concentration of hexane used in each experiment
 523 (0H, 20H, or 100H) and the corresponding chamber blanks (B).
 524

525 **Table 2: Chemical trends by selected mass range Groups I-IV for α -pinene ozonolysis SOA**

Parameter*	Group I < 300 n=140	300 < Group II < 475 n=294	475 < Group III < 650 n=314	650 < Group IV n=174
O:C Range	0.24 to 1.00	0.20 to 0.75	0.24 to 0.67	0.29 to 0.57
O:C Column Mean	0.55 \pm 0.19	0.46 \pm 0.12	0.43 \pm 0.09	0.42 \pm 0.06
H:C Range	1.14 to 1.86	1.25 to 1.86	1.30 to 1.69	1.38 to 1.65
H:C Column Mean	1.52 \pm 0.18	1.51 \pm 0.14	1.50 \pm 0.09	1.51 \pm 0.06
O:Sc Range	-1.20 to 0.67	-1.20 to 0.17	-1.04 to -0.10	-0.97 to -0.33
O:Sc Mean	-0.42 \pm 0.42	-0.58 \pm 0.29	-0.64 \pm 0.21	-0.68 \pm 0.14
# Oxygen Range	3 to 9	4 to 13	7 to 16	11 to 18
# Oxygen Mean (Median)	5.65 \pm 1.46 (6)	8.57 \pm 1.79 (9)	11.73 \pm 1.95 (12)	14.62 \pm 1.77 (15)
DBE Range	2 to 6	2 to 9	5 to 11	7 to 11
DBE Mean (Median)	3.55 \pm 1.11 (3)	5.65 \pm 1.47 (6)	7.84 \pm 1.42 (8)	9.65 \pm 1.08 (10)

526 *The parameters were calculated for each group without consideration of the analyte relative abundances. The ranges indicate
 527 the minimum and maximum values in each subset. The calculated means and their standard deviations demonstrate the
 528 distribution of values in each subset.
 529

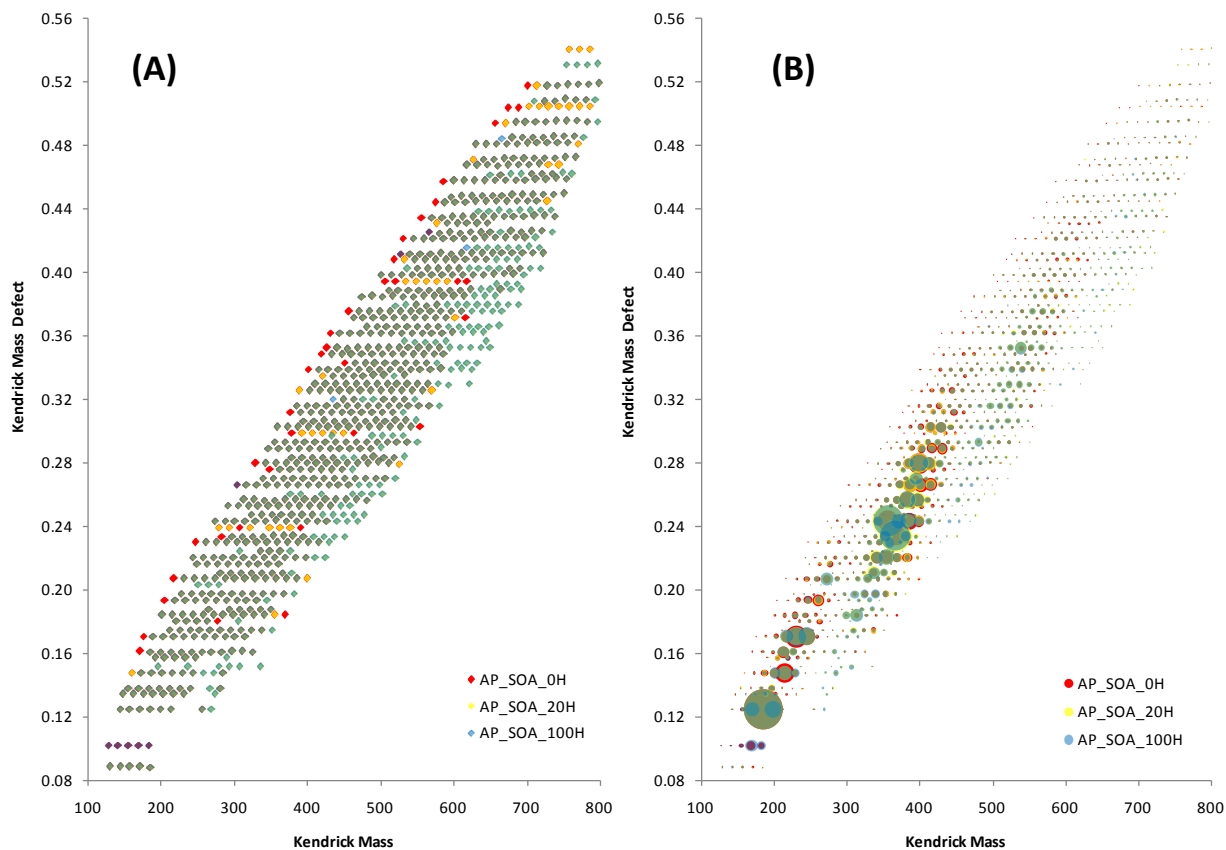
530 **Table 3: Relative abundance weighted ratios of O:C, H:C and OM:OC (this work and literature values)**

Sample ID	O:C _w	H:C _w	OM:OC _w
AP-SOA-0H	0.46 \pm 0.02	1.54 \pm 0.07	1.74 \pm 0.03
AP-SOA-20H	0.44 \pm 0.03	1.52 \pm 0.10	1.71 \pm 0.04
AP-SOA-100H	0.44 \pm 0.02	1.53 \pm 0.08	1.71 \pm 0.07
Isoprene SOA (Nguyen et al. 2010)	0.63 \pm 0.26	1.51 \pm 0.25	1.97 \pm 0.35
Limonene SOA (Bateman et al. 2009)	0.45 \pm 0.09	1.58 \pm 0.11	1.73 \pm 0.11

531 Weighted ratios indicated by X_w where X = O:C, H:C or OM:OC were done using the equations presented in Nguyen et al. 2010
 532

533

534 **Figures**
535



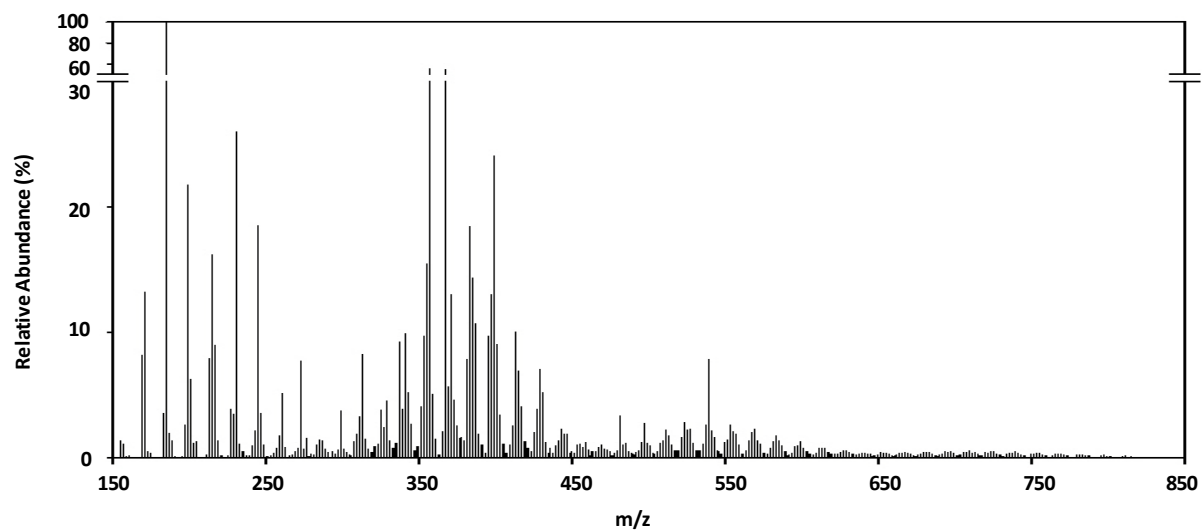
536

537 **Figure 1: Kendrick diagrams with semi-transparent primary colors for each experiment to illustrate the**
538 **unique and common formulas. Common analytes between any two experiments are shown with**
539 **green, orange and purple symbols and common analytes between all three experiments are brown (A)**
540 **an overlay of the three SOA experiments without relative abundance scaling; and (B) an overlay with**
541 **relative abundance corresponding to circle size. The relative abundances included here were the**
542 **calculated average of the replicate injections when available.**

543 *Note: This image requires color on the web and in print.*

544

545

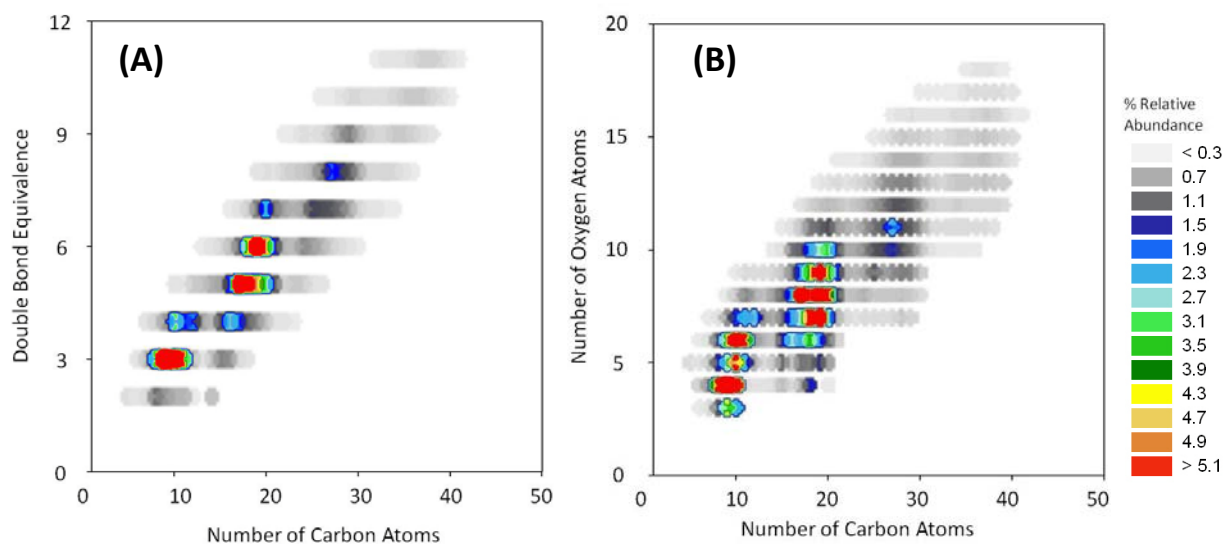


546

547 **Figure 2: Negative-ion ultrahigh-resolution FT-ICR mass spectra of the averaged α -pinene SOA with a**
548 **break in the y-axis between 30 and 60. The mass spectrum was reconstructed from the identified and**
549 **averaged monoisotopic peaks. Group I is all ions < 300 u, Group II is all ions between 300 and 475 u,**
550 **Group III is all ions between 475 and 650 u, and Group IV is all ions > 650 u. Additional mass spectra,**
551 **including those of the individual experiments are available in the supplemental information (Figure S-**
552 **1 and Figure S-2).**

553

554



555

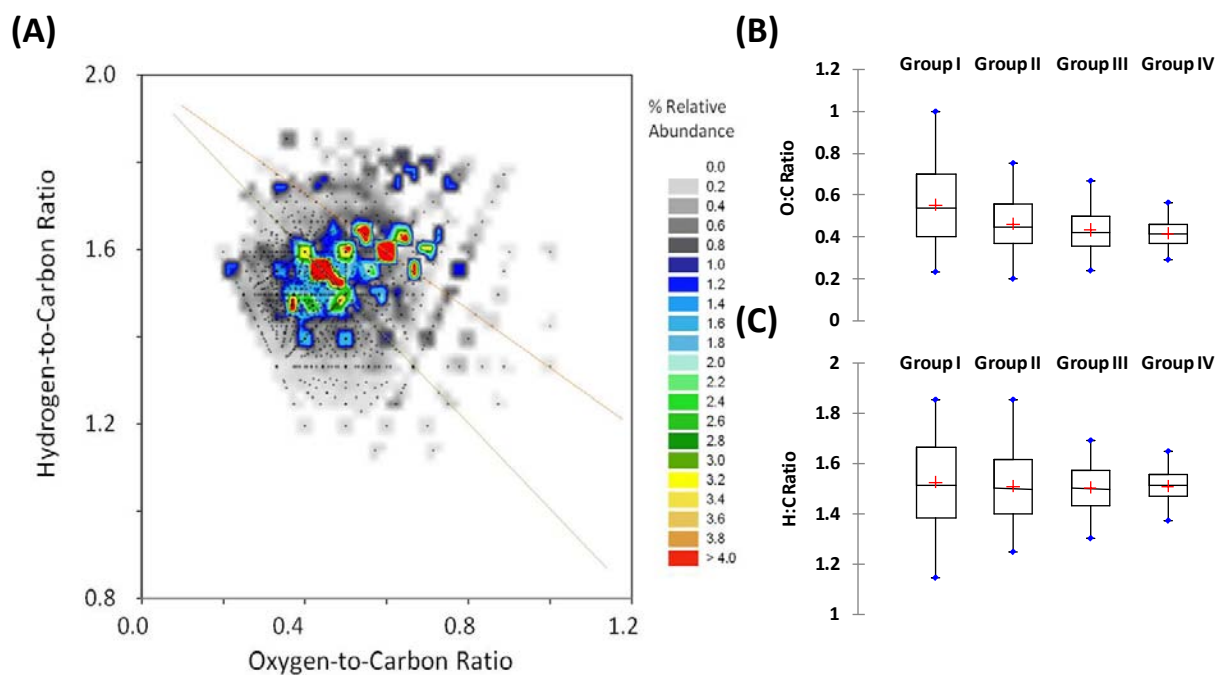
556 **Figure 3: Isoabundance plots for the averaged α -pinene SOA molecular formulas (A) DBE vs. the**
557 **number of carbon atoms in all chemical formulas; (B) The number of oxygen atoms vs. the number of**
558 **carbon atoms in all chemical formulas.**

559 *Note: This image requires color on the web and in print.*

560

561

562



563

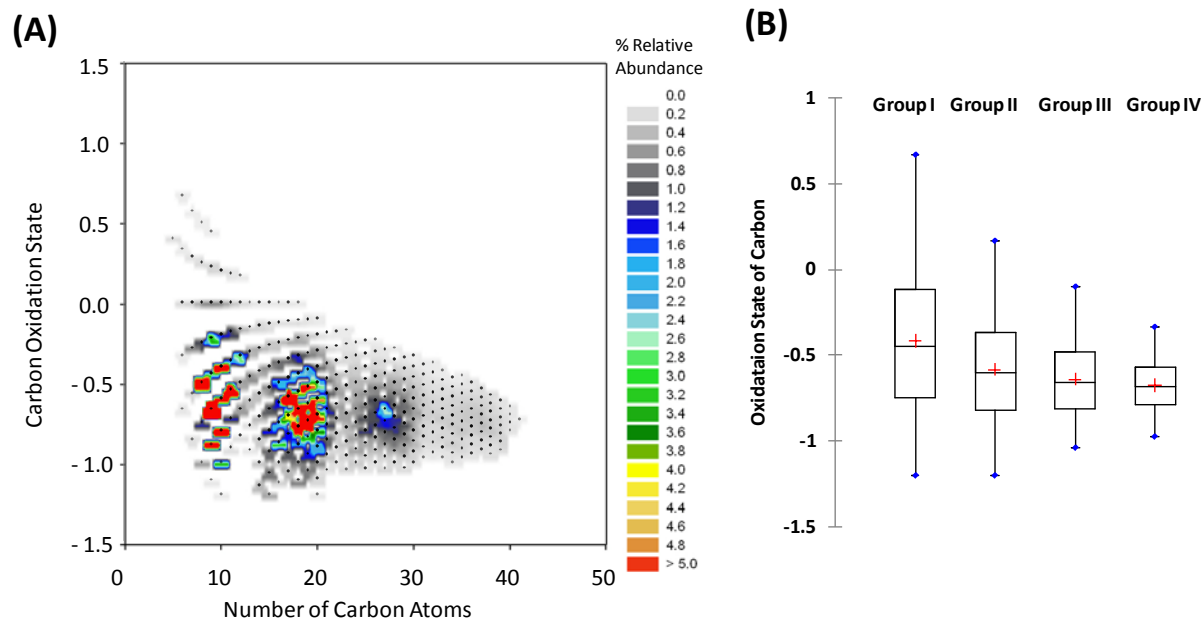
564 **Figure 4: Elemental composition characteristics (A) isoabundance van Krevelen diagram for the**
565 **averaged α -pinene SOA molecular formulas with the slopes equal to -1 and 0.7 illustrated with faint**
566 **green and orange lines; (B) box plots of the O:C ratios for the groups: Group I is all ions < 300 u, Group**
567 **II is all ions between 300 and 475 u, Group III is all ions between 475 and 650 u, and Group IV is all**
568 **ions > 650 u; and (C) box plots of the H:C ratios for the groups: Group I is all ions < 300 u, Group II is all**
569 **ions between 300 and 475, Group III is all ions between 475 and 650 u, and Group IV is all ions > 650 u.**

570

571 *Note: This image requires color on the web and in print.*

572

573



574

575 **Figure 5: Carbon oxidation states after Kroll *et al.* 2011 for the averaged α -pinene SOA molecular**
576 **formulas (A) isoabundance oxidation state plot and (B) box plots of the OS_c for the groups: Group I is**
577 **all ions < 300 u, Group II is all ions between 300 and 475, Group III is all ions between 475 and 650 u,**
578 **and Group IV is all ions > 650 u.**

579

580 *Note: This image requires color on the web and in print.*

581

582

583